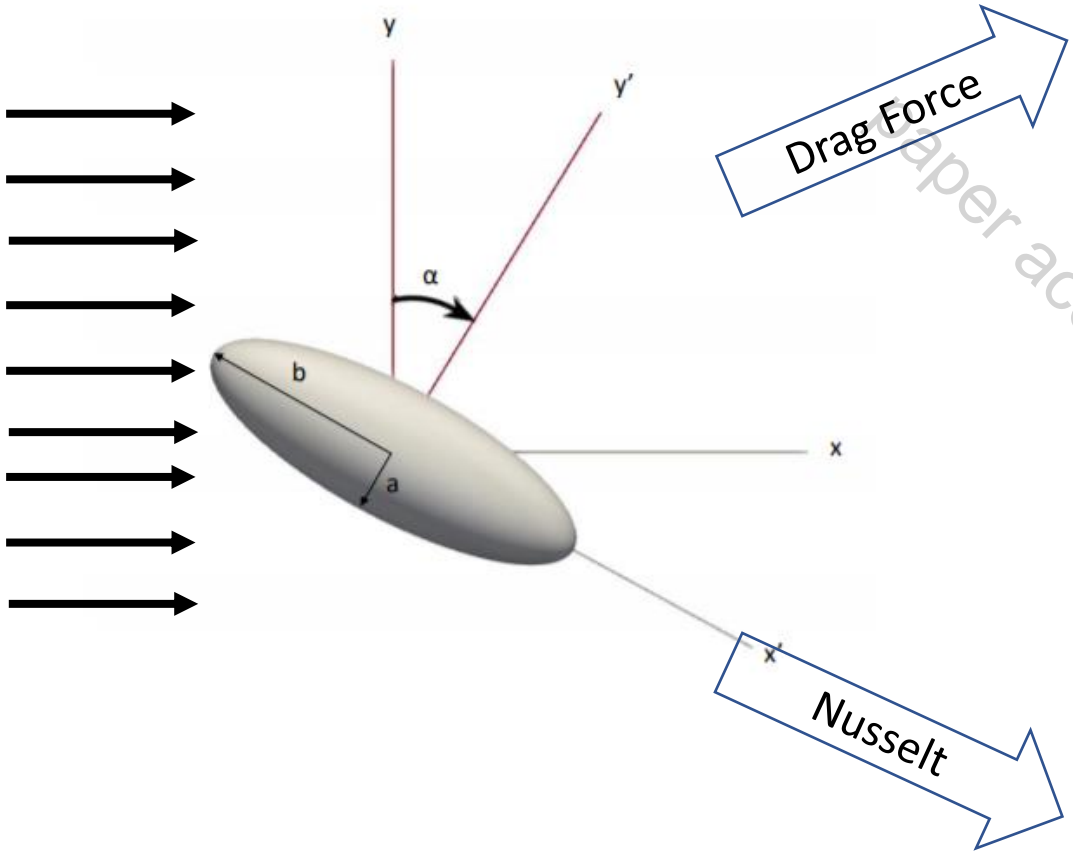

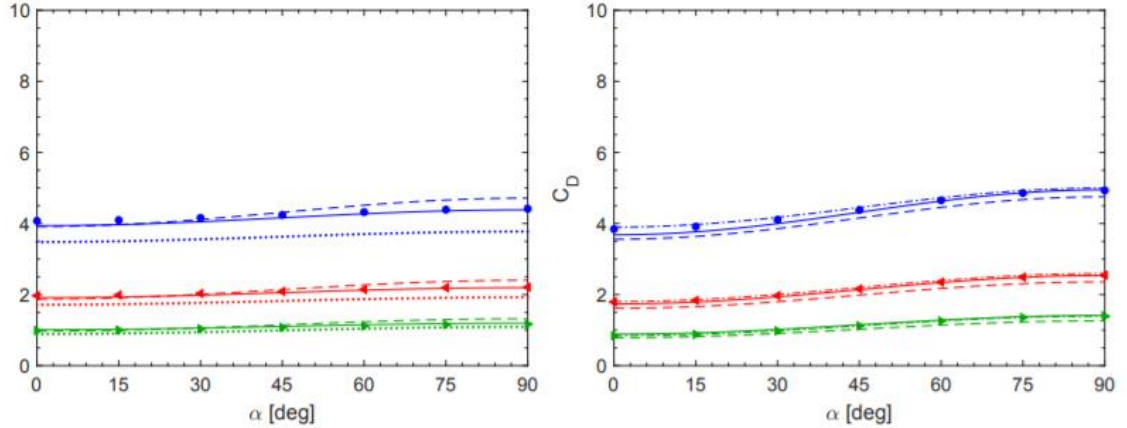

(a) $E = 1.25$ (b) $E = 2$

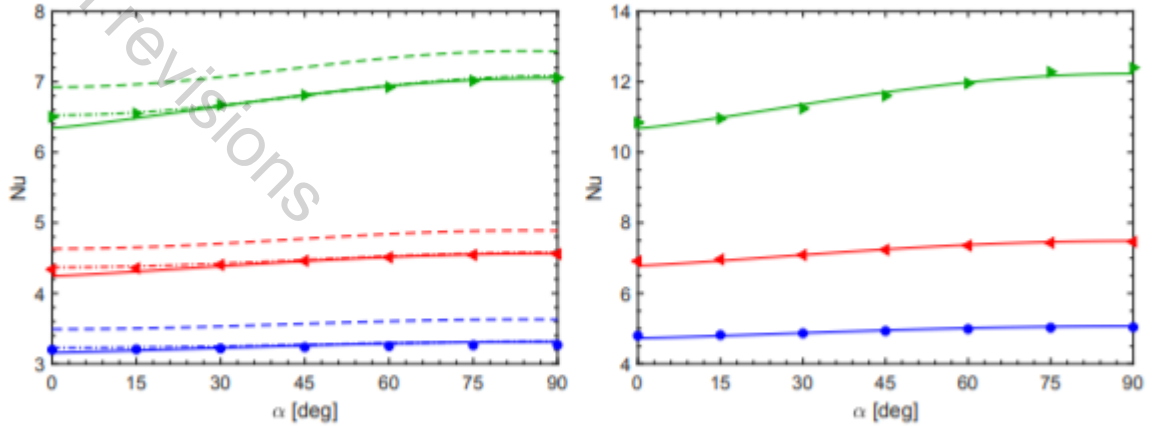

(a) $Pr = 0.7,\ E = 2$ (b) $Pr = 4,\ E = 2$

Abstract

In this work, numerical simulations at the particle scale were performed to determine the impact of the Reynolds number Re_p, the Prandtl number Pr, the aspect ratio of the particle E and the angle of attack α on the drag and lift forces, the pitching torque and the convective heat transfer coefficient for prolate spheroids in a steady flow. Validation cases have been studied to assess the accuracy of the present set-up including a polyhedral mesh. As a result, new correlations for drag, lift and pitching torque coefficients and Nusselt number have been derived. Compared to existing works, the present correlations are valid for wide range of aspect ratios ($1 \leq E \leq 10$) and Prandtl numbers ($0.7 \leq Pr \leq 7$).

On the determination of Nusselt number and hydrodynamic coefficients for prolate spheroids in a uniform steady flow

Alexandre Briclot, Mohammed Khalij, Boris Arcen, Anne Tanière

[a] *Université de Lorraine, CNRS, LEMTA, , Nancy, F-54000, , France*

Abstract

In this work, numerical simulations at the particle scale were performed to determine the impact of the Reynolds number Re_p, the Prandtl number Pr, the aspect ratio of the particle E and the angle of attack α on the drag and lift forces, the pitching torque and the convective heat transfer coefficient for prolate spheroids in a steady flow. Validation cases have been studied to assess the accuracy of the present set-up including a polyhedral mesh. As a result, new correlations for drag, lift and pitching torque coefficients and Nusselt number have been derived. Compared to existing works, the present correlations are valid for wide range of aspect ratios ($1 \leq E \leq 10$) and Prandtl numbers ($0.7 \leq Pr \leq 7$).

Keywords:

Prolate spheroids, Nusselt number, Hydrodynamic coefficients, Convective heat transfer

1. Introduction

Numerical simulations involving particle-laden flows are present in many industrial processes and are used to understand natural phenomena such as

the dispersion of volcanic ashes or pollutants [1]. In current models, the assumption of spherical particles is widely used to describe the interactions between the particles and the fluid [2, 3]. As a result, lift and torque effects are often underestimated while they can become important especially when the particles are ellipsoidal. Particles in industrial processes or in natural flows can have many different shapes and are rarely spherical. It is obviously impossible to develop a model for every shape of particle, therefore, they must be idealized to approach well-known shapes. It is then necessary to develop shape-dependent models to describe their motion and the heat transfer with the fluid.

In the Stokes regime ($Re_p \ll 1$), Jeffery [4] described the torques acting on ellipsoids in a shear flow and later, Happel and Brenner [5] determined the forces applied on an ellipsoid at low Reynolds number. Ganser [6] and Haider and Levenspiel [7] proposed an empirical drag correlation at higher Reynolds number for spherical and non-spherical particles. To do so, they used sphericity as a shape parameter which describes the ratio between the surface of the volume-equivalent sphere and the actual surface area of the particle. Unfortunately, it does not take into account the orientation of the particle. We now know that the angle of attack of a particle is a parameter that can greatly affect the hydrodynamic forces and heat transfer [8]. More recently, numerical investigations have been performed to determine the drag coefficient on arbitrary-shaped particles by Hölzer and Sommerfeld [8, 9] and on ellipsoids by Ouchene *et al.* [10], Zastawny *et al.* [11], Richter and Nikrityuk [12, 13], Sanjeevi *et al.* [14, 15] and Ke *et al.* [16]. In [10], [11], [13] and [14], the authors also developed lift and pitching torque correlations

for different types of prolate spheroids. However, these correlations are, most of the time, only applicable to certain aspect ratios noted E (ratio between the polar diameter and the equatorial diameter). Indeed, the correlations of Richter and Nikrityuk [13] are limited to an aspect ratio of 2, whereas those of Zastawny *et al.* [11] predict the hydrodynamic coefficients for prolate spheroids at $E = 1.25$ and $E = 2.5$. Only Ouchene *et al.* [10] performed numerical simulations for a very wide range of aspect ratios, from 1 to 32.

Regarding heat transfer, only Dwyer and Dandy [17], Richter and Nikrityuk [12, 13] and Ke *et al.* [16] worked on forced convection over prolate spheroids at moderate Reynolds numbers (Up to 250). Clift *et al.* [18] worked on spherical and deformed spheres including ellipsoids in slow viscous flows. As a result, the Nusselt number can only be estimated for a small part of ellipsoids. As for the hydrodynamic forces, the correlations of Richter and Nikrityuk [12, 13] are only valid for an ellipsoid whose aspect ratio is 2 while the one of Ke *et al.* [16] is valid for a range of aspect ratio from 0.25 to 2.5. Moreover, these two correlations describe the heat transfer from ellipsoids to the air at ambient temperature only, at $Pr = 0.7$.

It is now clear that the heat transfer from ellipsoids to other media than air is impossible to predict. To overcome this problem, we propose to investigate the evolution of the Nusselt number for spherical and ellipsoidal particles as a function of the Reynolds number, the Prandtl Number, the aspect ratio and the orientation of the particle. New correlations for the lift and pitching torque coefficients are also developed to extend the ranges of validity of the existing ones. Additionally, the correlation of Ouchene *et al.* [10] for the drag coefficient is refined to fit the present results. In the present work, we carried

out simulations for a range of Reynolds number from 0.1 to 100 and for Prandtl number values of 0.7, 1, 4 and 7. This covers a wide variety of fluids used in engineering processes like air and water at different temperatures. The aspect ratio varies between 1 and 10 and every angle of attack from 0° to 90° with a 15° step is considered.

2. Numerical overview

2.1. Governing equations

In this paper, the fluid is assumed to be Newtonian and incompressible, the fluid flow is considered as steady and the heating due to viscous effects is neglected. Therefore, the continuity, the Navier-Stokes and the energy equations can be written as :

$$\boldsymbol{\nabla} \cdot \mathbf{u} = 0, \tag{1}$$

$$(\mathbf{u} \cdot \boldsymbol{\nabla})\, \mathbf{u} = -\frac{1}{\rho}\boldsymbol{\nabla} p + \nu \boldsymbol{\nabla}^2 \mathbf{u}, \tag{2}$$

$$(\mathbf{u} \cdot \boldsymbol{\nabla})\, h = \frac{k}{\rho}\boldsymbol{\nabla}^2 T, \tag{3}$$

where $\mathbf{u}$ is the fluid velocity vector, ρ the fluid density, p the pressure, ν the kinematic viscosity, h the enthalpy, T the temperature and k the thermal conductivity of the fluid.

When dropped into a fluid, particles are subjected to forces that influence their motion. This can be described by Newton's second law [19] :

$$m_p \frac{\mathrm{d}\mathbf{u_p}}{\mathrm{d}t} = \sum \mathbf{F}, \tag{4}$$

where m_p denotes the mass of the particle, $\mathbf{u_p}$ its velocity and $\mathbf{F}$ the forces acting on it. Although many forces can be taken into account like gravitational, Brownian forces, etc., only drag and lift forces are considered here.

Torques acting on particles have two different origins. When the fluid and the particle do not have the same angular speed, a rotational torque is applied to the particle. In this paper, only the pitching torque is studied that occurs when the centre of pressure due to the resulting forces and centre of mass of the particle do not coincide. Rotational effects are described by Euler's rotation equations :

$$\mathbf{I}\frac{\mathrm{d}\boldsymbol{\omega_p}}{\mathrm{d}t} \; + \; \boldsymbol{\omega_p} \times (\mathbf{I}\boldsymbol{\omega_p}) \; = \; \mathbf{T}, \tag{5}$$

where $\mathbf{I}$ is the inertia tensor of the particle, $\boldsymbol{\omega_p}$ its angular velocity and $\mathbf{T}$ the applied torques. Equations 4 and 5 show that the forces and the torques acting on the particles have to be precisely determined to predict their motion. They are usually characterized by the dimensionless drag, lift and torque coefficients C_D, C_L and C_T respectively :

$$C_D = \frac{\|\mathbf{F_D}\|}{\frac{1}{2}\rho\|\mathbf{u_R}\|^2\pi\frac{d_p^2}{4}}, \qquad C_L = \frac{\|\mathbf{F_L}\|}{\frac{1}{2}\rho\|\mathbf{u_R}\|^2\pi\frac{d_p^2}{4}}, \qquad C_T = \frac{\|\mathbf{T}\|}{\frac{1}{2}\rho\|\mathbf{u_R}\|^2\pi\frac{d_p^3}{8}}. \tag{6}$$

These coefficients highly depend on the particle Reynolds number $Re_p = \frac{\|\mathbf{u_R}\|d_p}{\nu}$ where $\mathbf{u_R}$ denotes the relative velocity between the particle and the fluid and d_p is the volume-equivalent sphere diameter. If the particles are not spherical, their orientation and their shape also have an influence on the evolution of the hydrodynamic coefficients. For ellipsoidal particles, the orientation can be described by the angle of attack α which represents the angle between the major axis of the ellipsoid and the direction of the flow while the shape of the particle is determined by the aspect ratio $E = \frac{b}{a}$ (Fig. 1).

[Figure 1 about here.]

When the particle and the fluid are not at the same temperature, the variation of the particle temperature (that is considered uniform, i.e. $Bi \ll 1$) due to the convective heat transfer is described by :

$$m_p C_p \frac{\mathrm{d}T_p}{\mathrm{d}t} = h_c \; S \left(T_p - T_\infty\right), \tag{7}$$

where C_p, h_c, T_p and T_∞ respectively denote the specific heat capacity of the particle, the convective heat transfer coefficient, the temperature of the particle and the free-stream temperature of the fluid. The convective heat transfer coefficient can be related to the Nusselt number by the following relationship :

$$Nu = \frac{h_c \; d_p}{k}. \tag{8}$$

In addition to Re_p, α and E, the Nusselt number also depends on the Prandtl number $Pr = \frac{\nu}{\alpha_f}$, where α_f represents the thermal diffusivity of the fluid.

2.2. Numerical scheme and discretization

For this study, the three-dimensional Navier-Stokes equations with heat transfer are solved using the commercial software Ansys FLUENT to determine the particle-scale velocity, pressure and temperature fields. The pressure-velocity coupling problem is solved using the SIMPLE (Semi-Implicit Method for Pressure-Linked Equations) algorithm. This way, the pressure is corrected by the velocity field and the mass conservation is forced. The interpolation of cell-centred values to face-centred values is accomplished using a second order Upwind scheme to limit numerical diffusion.

Only forced convection is considered here so that the temperature acts as a passive scalar, thus the energy equation can be solved independently of the Navier-Stokes equation.

The numerical simulations stop when the convergence of each of the hydrodynamics coefficients C_D, C_L and C_T and the Nusselt number reaches 10^{-6}, i.e. when $\frac{|X^i - X^{i-1}|}{X^i} < 10^{-6}$, where X^i represents the value of the studied quantity at the i-th iteration.

The size of the computational domain is $140d_p \times 80d_p \times 80d_p$. These dimensions have been determined to ensure that the boundary layer is captured even at very low Reynolds number [10]. In addition, the length of the box is sufficient for the development of the wake behind the particle. The centre of the particle is located at the centre of the yz-plane, $35d_p$ away from the inlet and corresponds to the origin of the axes (see Fig. 2). The non-conformal mesh consists of two different parts. Close to the particle, the mesh is unstructured and composed of polyhedral cells and a 35-layer inflation while far from the prolate spheroid, it is structured in hexahedral cells (see Fig. 3). The size of the inner domain adapts to the size of the particle to capture the boundary layer (except for the Stokes regime where the boundary layer becomes very large, as it grows like $\sim 1/Re_p$) while the outer domain does not change.

Polyhedral meshes have been chosen as they decrease the number of cells in the domain, merging several tetrahedral cells together and have a better quality (skewness and smoothness). As a result, they usually allow a faster convergence and decrease the computational time. Moreover, gradients can be approximated with a better accuracy with polyhedral cells than tetrahedral ones due to their high number of neighbours. According to Perić [20], polyhedral meshes are particularly good when dealing with recirculating flows. For this reason, we used polyhedral cells close to the particle to

capture the recirculating zone behind it.

[Figure 2 about here.]

[Figure 3 about here.]

2.3. Boundary conditions

The prolate spheroid, whose surface temperature is assumed to be constant is immersed in a cross-flow so that the temperature difference between the surface of the particle and the fluid is 100K. At the inlet, the velocity and the temperature are constant and equal to the free stream conditions. At the outlet, constant pressure and temperature conditions are applied while a symmetry condition (i.e. zero gradient condition) is set at the other boundaries for velocity, pressure and temperature (see Fig. 2). These conditions write as :

- At the inlet

$$V_x = V_\infty,$$
$$V_y = V_z = 0,$$
$$T = T_\infty = 300K,$$

- At the outlet

$$\frac{dP}{dx} = 0,$$
$$\frac{dT}{dx} = 0,$$

- At the surface of the particle

$$T_p = 400K,$$
$$V_x = V_y = V_z = 0,$$

- Other boundaries

$$\frac{dV}{dy} = \frac{dV}{dz} = 0,$$
$$\frac{dT}{dy} = \frac{dT}{dz} = 0,$$
$$\frac{dP}{dy} = \frac{dP}{dz} = 0.$$

2.4. Mesh independence

Three different polyhedral meshes and their associated tetrahedral meshes were tested to validate the current set up (see Table 1). The use of polyhedral meshes reduces the number of cells by up to 30% and the CPU time by 35% to 50% compared to associated tetrahedral meshes (32 cores were used in each case). The variations of C_D and Nu as a function of the number of cells are not significant and can be considered negligible between grids 1T-2T and 1P-2P. Moreover, no significant differences on C_D and Nu are observed between polyhedral and tetrahedral meshes but the first ones converge faster. Finally, the grid 2P has been chosen as it offers a good precision and better computational performances than other grids.

[Table 1 about here.]

3. Validation cases

As polyhedral meshes have never been used to simulate flows over single particles, it is necessary to ensure the accuracy of the results. To do so, the behaviour of a sphere immersed in a flow at different Reynolds number was first studied. In a second time, ellipsoids in Stokes flows were considered and the results for the hydrodynamic coefficients and the Nusselt number are compared to the analytical and empirical correlations previously cited.

3.1. Flow past a sphere

Concerning the drag coefficient, the results of the present study (up to $Re_p = 100$) are compared to the correlations of Schiller and Naumann [21], Morsi and Alexander [22] and Haider and Levenspiel [7]. It can be seen from

table 2 and figure 4 that the present results are in very good accordance with the correlation of Schiller and Naumann [21] since the maximum relative error does not exceed 3.5%. The error compared to the correlations of Haider and Levenspiel [7] and Morsi and Alexander [22] is slightly higher but is still reasonable. At very low Reynolds numbers, the computed drag coefficients tend to the theoretical solution of Stokes [23] $\frac{24}{Re_p}$ with a good accuracy; at $Re_p = 0.1$ the relative deviation is about 0.6%.

[Table 2 about here.]

[Figure 4 about here.]

The evaluations of the Nusselt number for a sphere ($Re_p \leq 100$ and $Pr \leq 7$) are compared to the correlations of Clift *et al.* [18], Ranz and Marshall [24] and Whitaker [25]. The first one describes our results with a very small deviation while a larger error can be observed compared to [24] and [25] as it is shown in table 3. Richter and Nikrityuk [12] and Bagchi [26] noted that the correlations of Ranz and Marshall [24] and Whitaker [25] respectively overestimated and underestimated their data concerning the heat transfer to the air, corresponding to a Prandtl number of 0.7. The same observation can be made here at $Pr = 0.7$ and $Pr = 1$ (see Fig. 5). For Prandtl numbers of 4 and 7, both the correlations from [24] and [25] underestimate the computed Nusselt numbers while the correlation of Clift *et al.* still fits them very well.

[Table 3 about here.]

[Figure 5 about here.]

3.2. Flow past an ellipsoid at low Reynolds number

Secondly, simulations have been run at $Re_p = 0.1$ for each aspect ratio. The drag and lift coefficients are compared to the theoretical results given by Happel and Brenner [5] (see Fig. 6) and the Nusselt number to the correlation of Clift *et al.* [18]. The present simulations slightly overestimates the force coefficients but the deviations from the results given by Happel and Brenner [5] are very small for both of them as it is presented in table 4. However, it seems that the relative error increases with the aspect ratio up to 2.5 % for C_D and 5.4% for C_L when $E = 10$. It is possible that the aspect ratio has an impact on the upper bound of the Stokes regime and that the common bound $Re_p < 0.1$ is not the only criterion to take into account.

[Table 4 about here.]

[Figure 6 about here.]

In creeping flows, the angle of attack does not have any influence on the heat transfer as the convection effects are negligible, thus only E, Re_p and Pr affect Nu. It has been shown in [18] that the Reynolds number and the Prandtl number are equally important and are regrouped as the Peclet number, $Pe = Re_p\ Pr$. The deviations from the correlation proposed by Clift *et al.* [18] increase up to 4.1% with the Peclet number as it is shown in table 5. Nonetheless, the results for the Nusselt number are quantitatively close to the predicted values. Whatever the value of the Prandtl number, the error also increases with the aspect ratio for the same reason as the deviations

concerning force coefficients increase (not shown here).

[Table 5 about here.]

In this section, we have seen that the present set-up is accurate enough to simulate heat and fluid flows past spheres and ellipsoids for a large range of Reynolds number and different Prandtl numbers. The evolution of the drag and lift coefficients with the angle of attack is well predicted for each aspect ratio studied in the Stokes regime. The Nusselt number is in good accordance with the correlation of Clift *et al.* [18] for both spheres and ellipsoids. The domain size is sufficient to model the boundary layer in creeping flows as well as the wake in higher Reynolds-number flows. The local use of polyhedral meshes allowed to run several simulations keeping the simulation costs low.

4. Results

In this section, a new correlation is developed to describe the evolution of the Nusselt number as a function of the Reynolds number, the Prandtl number, the aspect ratio and the angle of attack of the particle. On the other hand, the correlation for drag of Ouchene *et al.* [10], corrected later in Arcen *et al.* [27] due to typos, is refined to fit the present results and two new correlations for the lift and pitching torque coefficients are presented.

4.1. Nusselt number

According to previous works dealing with spheres, the evolution of the Nusselt number can be described as multiple functions of Re_p and Pr. Now,

because of the asymmetry of ellipsoidal particles, the shape and the orientation have to be taken into account. Following the work of Richter and Nikrityuk [13] and Ke *et al.* [16], the effects of the angle of attack on the Nusselt number can be reasonably approximated by a power of the sine function. Based on this observation, the following form for the Nusselt number is sought :

$$Nu = Nu_0 + (Nu_{90} - Nu_0)\ sin^a(\alpha), \tag{9}$$

where Nu_0 and Nu_{90} respectively denote the Nusselt number at 0° and 90°. Both Nu_0 and Nu_{90} evolve as functions of Re_p, Pr, and E. Two additional criteria are important for the development of the new correlation :

- When $Re_p \to 0$, the solution has to approach the theoretical value of the Nusselt number in a stagnant flow given by Clift *et al.* [18] $Nu_s = \frac{d_p C}{S}$ where S is the surface of the particle and C is the conductance defined, for a prolate spheroid by :

$$C = \frac{2\pi d_p E^{1/3}\sqrt{E^2-1}}{\ln\left(E+\sqrt{E^2-1}\right)}, \tag{10}$$

  It is worth noting that $Nu_s \to 2$ when $E \to 1$ which is a well-known result.

- When $E \to 1$, both Nu_0 and Nu_{90} have to converge towards the same value.

Based on these criteria and using a least squares regression, the following correlation is obtained :

$$
\begin{aligned}
&Nu = Nu_0 + (Nu_{90} - Nu_0)\ \sin^{1.20}(\alpha),\\
&Nu_0 = Nu_s + 0.65Re_p^{0.35}Pr^{0.21} + 0.51Re_p^{0.49}Pr^{0.35}E^{-0.27} - 0.84Re_p^{0.23}E^{-0.15},\\
&Nu_{90} = Nu_0 + 0.15Re_p^{0.66}Pr^{0.45}(E^{0.34} - 1).
\end{aligned}
\tag{11}
$$

This correlation is valid as long as $Re_p \leq 100$, $0.7 \leq Pr \leq 7$ and $1 \leq E \leq 10$. Taking into account all the results from our work, the mean and the maximum relative deviations between the simulations and the Nu correlation are respectively 1.14% and 5.30% (see Table 6 for more details). As this correlation degenerates to the theoretical value of the Nusselt number in a stagnant flow, its range of validity can be extended to $Re_p \to 0$. Compared to existing works ([12] [13] [16]), the present correlation has a large range of validity, especially in terms of Prandtl numbers and aspect ratios. To our knowledge, no works have been done on heat transfer for ellipsoids whose aspect ratio is higher than 3 nor for Prandtl number higher than 0.7.

In contrast to Richter and Nikrityuk [13] and Ke *et al.* [16], we found out that the best exponent of the $\sin(\alpha)$ term is not 2. Although it is sufficient for low aspect ratio prolate spheroids, when the particles become more elongated, the power of the sine function decreases. Actually, the exponent depends on the Reynolds number, the Prandtl number and the aspect ratio. For the sake of simplicity, the interpolation between 0° and 90° is done by a single coefficient that turns out to be 1.20. This value has been determined to minimize the error between the numerical results and the regression model, considering that the amplitude of the quantity $(Nu_{90} - Nu_0)$ increases with

E. A comparison of the present correlation and results from Richter and Nikrityuk [13] ($Re_p \leq 250$, $Pr = 0.7$ and $E = 2$) and Ke *et al.* [16] ($Re_p \leq 200$, $Pr = 0.7$ and $E \leq 2.5$) is presented in figure 7a and in table 6. The correlation of Ke *et al.* [16] slightly overestimates the present results while the one of Richter and Nikrityuk [13] fits our data precisely. It can be seen that the sine-squared interpolation gives better results at $E = 2$ but the function $\sin^{1.20}(\alpha)$ is more accurate for larger aspect ratios.

[Table 6 about here.]

[Figure 7 about here.]

While the Reynolds and the Prandtl numbers determine the mean value of the Nusselt number over the range of angles of attack, the major impact of the aspect ratio on the Nusselt number is through the magnitude of the quantity $(Nu_{90} - Nu_0)$. Comparing figures at $E = 2$ with the figures at $E = 10$, it can be seen that the curves are centred around the same value but the deviation to the mean is 4 to 8 times larger at $E = 10$ than at $E = 2$.

4.2. Drag coefficient

In creeping flows, Happel and Brenner [5] showed that the evolution of the drag coefficient as a function of the angle of attack follows the function $\sin^2(\alpha)$ between 0° and 90°. Ouchene *et al.* [10], Zastawny *et al.* [11], Ke *et al.* [16] and Richter and Nikrityuk [13] observed the same evolution of the drag coefficient, even at higher Reynolds number. This behaviour has also been reported for the mean drag coefficients in unsteady flows by Sanjeevi *et al.* [14] at $Re_p = 2000$. In figure 8, the data of every case studied are

reported and compared to the function $\sin^2(\alpha)$. Whatever the values of the Reynolds number and the aspect ratio, the curve fits all the data points with very small deviations. As a result, a new correlation is developed based on the generic form :

$$C_D = C_{D0} + (C_{D90} - C_{D0})\ \sin^2(\alpha). \tag{12}$$

Following the work of Ouchene *et al.* [10], the form of the correlation is preserved but the coefficients are refined to fit the present results.

$$\begin{aligned} C_{D0} &= \frac{24}{Re_p}\left[K_0 + 0.15E^{-0.44}Re_p^{0.687} + \frac{E^{-1.69}(E-1)^{2.23}}{24}Re_p^{0.49}\right], && Re_p \leq 100 \\ C_{D90} &= \frac{24}{Re_p}\left[K_{90} + 0.15Re_p^{0.687} + \frac{E^{0.12}(E-1)^{0.77}}{24}Re_p^{0.72}\right], && 1 \leq E \leq 10 \end{aligned} \tag{13}$$

where K_0 and K_{90} are the correction factors of Happel and Brenner [5] defined for prolate spheroids by :

$$K_0 = \frac{8}{3}E^{-1/3}\left[-\frac{2E}{E^2-1} + \frac{2E^2-1}{(E^2-1)^{3/2}}\ln\left(\frac{E+\sqrt{E^2-1}}{E-\sqrt{E^2-1}}\right)\right]^{-1}, \tag{14}$$

$$K_{90} = \frac{8}{3}E^{-1/3}\left[\frac{E}{E^2-1} + \frac{2E^2-3}{(E^2-1)^{3/2}}\ln\left(E+\sqrt{E^2-1}\right)\right]^{-1}. \tag{15}$$

When $E = 1$, the correlation of Schiller and Naumann [21] is retrieved and when $Re_p \to 0$, the correlation tends towards theoretical results of Happel and Brenner [5]. As a result, the range of validity of the present correlation can be extended, just like the present Nu correlation to $Re_p \to 0$.

[Figure 8 about here.]

[Figure 9 about here.]

[Table 7 about here.]

The relative deviation between the results of simulations and the present correlation does not exceed 5.04% (see table 7). Like the Nu correlation, the mean error does not vary much as the aspect ratio increases which means that the correlation is equally good for each shape studied here. Maximum deviations occur when $Re_p = 0.1$ or $Re_p = 100$. Although the correlation tends towards the correlation of Happel and Brenner [5], the last term in C_{D0} and C_{D90} can introduce a small deviation at small but finite Re_p, especially when the aspect ratio increases.

Our results are sensibly equal to the results from Richter and Nikrityuk [13] for $Re_p \geq 10$ and $E = 2$ while a larger error is noticed when compared to the work of Zastawny *et al.* [11]. At low aspect ratios, the correlation of Ouchene *et al.* [10] gives results similar to ours as it can be seen in figure 9. The relative deviations increase with E, particularly at $\alpha = 90°$ as it has also been noticed by Sanjeevi *et al.* [14]. Because of the form of the C_D correlation, the large error in C_{D90} has a direct impact on the results at other angles of attack so that the overall mean deviation is about 11.5%.

Compared to the work of Richter and Nikrityuk [13] and Zastawny *et al.* [11], the present correlation represents a significant improvement concerning the range of validity in term of the aspect ratio. A large improvement has also been made on the accuracy of the results compared to Ouchene *et al.* [10].

4.3. Lift Coefficient

In the Stokes regime, the lift coefficient can be determined from the drag coefficient according to Happel and Brenner [5] :

$$C_L^S = (C_{D90} - C_{D0})\ \sin(\alpha)\ \cos(\alpha). \tag{16}$$

In slow viscous flows, the lift coefficient has a symmetric behaviour at 45° while the symmetry breaks at higher Reynolds number. For elongated particles, the maximum C_L is shifted to higher angles of attack. This phenomenon is not totally understood and to our knowledge, no studies have been done on the location of maximum lift coefficient as functions of Re_p and E. To take this asymmetry into account, Zastawny *et al.* [11] and Sanjeevi *et al.* [14] added two corrective factors as exponents of the sine and cosine terms that only depend on the Reynolds number, as they studied only specific values of E. In the same way, Ouchene *et al.* [10] added a single exponent on the sine term depending on Re_p only. We found out that E plays a role as important as Re_p in the skewness of the lift profile. Indeed, comparing figures 10a and 10d, it can be seen that the lift profile is much more skewed at $E = 10$ than at $E = 1.25$ when $Re_p = 100$. The same observation can be noted comparing the curves at $Re_p = 10$ and $Re_p = 100$. Moreover, as the dependence on C_D is no longer obvious, the $(C_{D90} - C_{D0})$ term is replaced by C_{L45} :

$$C_L = \left(\frac{2}{\sqrt{2}}\right)^{1+F} C_{L45}\ \cos(\alpha)\ \sin^F(\alpha), \qquad \begin{matrix} Re_p \leq 100 \\ 1 \leq E \leq 10 \end{matrix} \tag{17}$$

with,

$$\begin{cases} F = 1 + 0.0129(Re_p E)^{0.5}, \\ C_{L45} = C_{L45}^S \left[1 + b_1 E^{b_2} Re_p^{b_3} + Re_p\ e^{\left(-b_4 E^{b_5} Re_p^{b_6}\right)}\right], \end{cases}$$

where C_{L45}^{S} denotes the lift coefficient at 45° determined from the equation (16). The six coefficients b_n are obtained by surface-fitting the present results :

$$b_1 = 0.14064 \quad b_2 = -0.34973 \quad b_3 = 1.0778$$
$$b_4 = 1.4300 \quad b_5 = -0.8860 \quad b_6 = 0.23938$$

The present correlation is equivalent to the theoretical correlation of Happel and Brenner [5] when $Re_p \to 0$ so that its range of validity is extended to low values of Re_p. Due to the complexity of the lift behaviour and the low values of C_L, the relative deviations between the present results and the correlation are higher than those of C_D (see table 8).

Large errors are noted between the present correlation and the results from the correlation of Ouchene *et al.* [10] and they increase with increasing E. However, it can be seen from figures 10a and 10b that the correlations of Zastawny *et al.* [11] and Richter and Nikrityuk [13] are in good accordance with ours. On the other hand, the correlation from Ouchene *et al.* [10] gives results that are qualitatively similar to ours but quantitatively different. This difference becomes more pronounced as the Reynolds number increases.

[Figure 10 about here.]

[Table 8 about here.]

4.4. Pitching torque coefficient

The behaviour of the pitching torque is very similar to that of lift but the asymmetry at high Re_p and high E is less pronounced. For this reason, the form of the correlation associated with the pitching torque coefficient is

exactly the same as the lift correlation (Eq. (17)). However, there exists no theoretical formulation for the pitching torque in creeping flows. Hence, the determination of C_{T45} is purely based on our numerical work and does not tend to any theoretical value when $Re_p \to 0$. The range of validity of the present correlation then starts at $Re_p = 0.1$.

$$C_T = \left(\frac{2}{\sqrt{2}}\right)^{1+F} C_{T45}\ \cos(\alpha)\ \sin^F(\alpha), \qquad \begin{array}{l} 0.1 \le Re_p \le 100 \\ 1 \le E \le 10 \end{array} \tag{18}$$

with,

$$\begin{cases} F = 1 + 5.136 \times 10^{-8}\,(Re_p E)^{2.141}\,, \\ C_{T45} = E^{c_1}\ln(E)\dfrac{c_2 + c_3 Re_p^{c_4} E}{c_5 + Re_p E} + c_6 \ln(E)^{c_7} Re_p^{c_8}, \end{cases}$$

where the coefficients c_n were determined to fit the present results :

$$\begin{array}{llll} c_1 = 1.218 & c_2 = 3.114 & c_3 = 0.05427 & c_4 = 0.2344 \\ c_5 = 11.28 & c_6 = 0.8311 & c_7 = 0.9235 & c_8 = -0.09705 \end{array}$$

The overall mean deviation between the results of simulations and the correlation is about 2.22% (see Table 9) which is very similar to that of C_L. The results from Richter and Nikrityuk [13] are, again, very close to ours with a maximum deviation of 1.34%. On the other hand, large deviations are noted when compared to the results of Ouchene *et al.* [10] which is not surprising as discrepancies have also been reported for C_D and C_L.

[Table 9 about here.]

[Figure 11 about here.]

Conclusion

The determination of the hydrodynamic forces and the convective heat transfer coefficient are essential to predict the motion of the particles and the heat transfer between the particles and the fluid. Some correlations for the drag, lift and pitching torque coefficients and the Nusselt number at the particle scale already exist in the literature but their ranges are very limited. Motivated by this fact, numerical simulations have been performed for a wide range of Reynolds numbers, Prandtl numbers, angles of attack and aspect ratios. The use of a partial polyhedral mesh allowed a considerable gain in time so that a large amount of data have been collected. The accuracy of the present simulations has been correctly verified through validation cases. Indeed, reference results for Nu, C_D and C_L for ellipsoidal particles in creeping flow and spheres are retrieved with very low errors.

As a result, Nu, C_D, C_L and C_T correlations have been derived for aspect ratios between 1 and 10 and Prandtl numbers between 0.7 and 7. Concerning the drag and the lift forces and the Nusselt number, the present correlations tend to theoretical solutions when $Re_p \to 0$ so that their range of validity has no lower limit. Unfortunately, the lack of theoretical work concerning the pitching torque for ellipsoidal particles did not allow the same extension at low Reynolds number. However, the present correlations are valid up to $Re_p = 100$ and for all angles attack by rotational symmetry.

Moreover, the results of the present correlations are in very good accordance with our results of simulations as the maximum relative errors are 5.30%, 5.04 %, 10.0% and 9.33% respectively for Nu, C_D, C_L, C_T. Our work is also in agreement with the ones of Richter and Nikrityuk [12, 13] for all the

hydrodynamic coefficients and the Nusselt number at $E = 2$ and $Pr = 0.7$ while large discrepancies have been noted when compared to the work of Zastawny *et al.* [11] and Ouchene *et al.* [10].

These correlations can be directly implemented in a Eulerian-Lagrangian simulation code to track the particles and study their dispersion as well as the convective heat transfer from the particles to the fluid.

References

[1] Y. Tominaga, T. Stathopoulos, CFD simulation of near-field pollutant dispersion in the urban environment: A review of current modeling techniques, Atmospheric Environment 79 (2013) 716–730.

[2] C. Marchioli, A. Soldati, J. Kuerten, B. Arcen, A. Taniere, G. Goldensoph, K. Squires, M. Cargnelutti, L. Portela, Statistics of particle dispersion in direct numerical simulations of wall-bounded turbulence: results of an international collaborative benchmark test, International Journal of Multiphase Flow 34 (2008) 879–893.

[3] F. Picano, W. Breugem, L. Brandt, Turbulent channel flow of dense suspensions of neutrally-buoyant spheres, Journal of Fluid Mechanics 764 (2015) 463–487.

[4] G. B. Jeffery, The motion of ellipsoidal particles immersed in a viscous fluid, Proc. R. Soc. Lond. 102 (1922) 161–179.

[5] J. Happel, H. Brenner, Low Reynolds Number Hydrodynamics, Prentice Hall, 1965.

[6] G. H. Ganser, A rational approach to drag prediction of spherical and nonspherical particles, Powder Technology 77 (1993) 143–152.

[7] A. Haider, O. Levenspiel, Drag coefficient and terminal velocity of spherical and nonspherical particles, Powder Technology 58 (1989) 63–70.

[8] A. Hölzer, M. Sommerfeld, New simple correlation formula for the drag coefficient of non-spherical particles, Powder Technology 184 (2008) 361–365.

[9] A. Hölzer, M. Sommerfeld, Lattice boltzmann simulations to determine drag, lift and torque acting on non-spherical particles, Computers and Fluids 38 (2009) 572–589.

[10] R. Ouchene, M. Khalij, B. Arcen, A. Tanière, A new set of correlations of drag, lift and torque coefficients for non-spherical particles and large reynolds numbers, Powder Technology 303 (2016) 33–43.

[11] M. Zastawny, G. Malloupas, F. Zhao, B. Wachem, Derivation of drag and lift force and torque coefficients for non-spherical particles in flows, Int. J. of Multiphase Flow 39 (2012) 227–239.

[12] A. Richter, P. Nikrityuk, Drag forces and heat transfer coefficients for spherical, cuboidal and ellipsoidal particles in cross flow at sub-critical reynolds numbers, Int. J. of Heat and Mass Transfer 55 (2012) 1343–1354.

[13] A. Richter, P. Nikrityuk, New correlations for heat and fluid flow past ellipsoidal and cubic particles at different angles of attack, Powder Technology 249 (2013) 463–474.

[14] S. Sanjeevi, J. Kuipers, J. T. Padding, Drag, lift and torque correlations for non-spherical particles from stokes limit to high reynolds numbers, Int. J. of Multiphase Flow 106 (2018) 325–337.

[15] S. Sanjeevi, J. T. Padding, On the orientational dependence of drag experienced by spheroids, J. Fluid Mech. 820 (2017) R1.

[16] C. Ke, S. Shu, H. Zhang, H. Yuan, D. Yang, On the drag coefficient and averaged nusselt number of an ellipsoidal particle in a fluid, Powder Technology 325 (2018) 134–144.

[17] H. A. Dwyer, D. Dandy, Some influences of particle shape on drag and heat transfer, Physics of Fluids A: Fluid Dynamics 2 (12) (1990) 2110–2118.

[18] R. Clift, J. Grace, M. Weber, Bubbles, Drops and Particles, Academic Press, 1978.

[19] M. Maxey, J. Riley, Equation of motion for a small rigid sphere in a nonuniform flow, The Physics of Fluids 26 (4) (1983) 883–889.

[20] M. Perić, Flow simulation using control volumes of arbitrary polyhedral shape, ERCOFTAC Bulletin 62 (2004) 25–29.

[21] L. Schiller, Z. Naumann, A drag coefficient correlation, Zeitschrift des Vereins Deutscher Ingenieure 77 (1935) 318–320.

[22] S. Morsi, A. Alexander, An investigation of particle trajectories in two-phase flow system, J. Fluid Mech. 55 (1972) 193–208.

[23] G. G. Stokes, On the effect of the inertial friction of fluids on the motion of pendulums, Trans. Cambridge Phil. Soc. 9 (1851) 8–23.

[24] W. Ranz, W. Marshall, Evaporation from drops, Chem. Eng. Progress 48 (1952) 173–180.

[25] S. Whitaker, Forced convection heat transfer correlations for flow in pipes, past flat plates, single cylinders, single spheres, and for flow in packed beds and tube bundles, AIChE Journal 18 (1972) 361–371.

[26] P. Bagchi, M. Ha, S. Balachandar, Direct numerical simulation of flow and heat transfer from a sphere in a uniform cross-flow, Journal of Fluids Engineering 123 (2001) 347–358.

[27] B. Arcen, R. Ouchene, M. Khalij, A. Tanière, Prolate spheroidal particles' behavior in a vertical wall-bounded turbulent flow, Physics of Fluids 29 (2017) 093301.

List of Figures

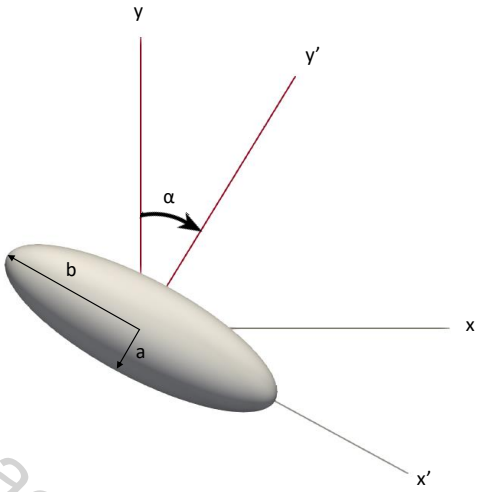

Figure 1 : Characterisation of a prolate spheroid.

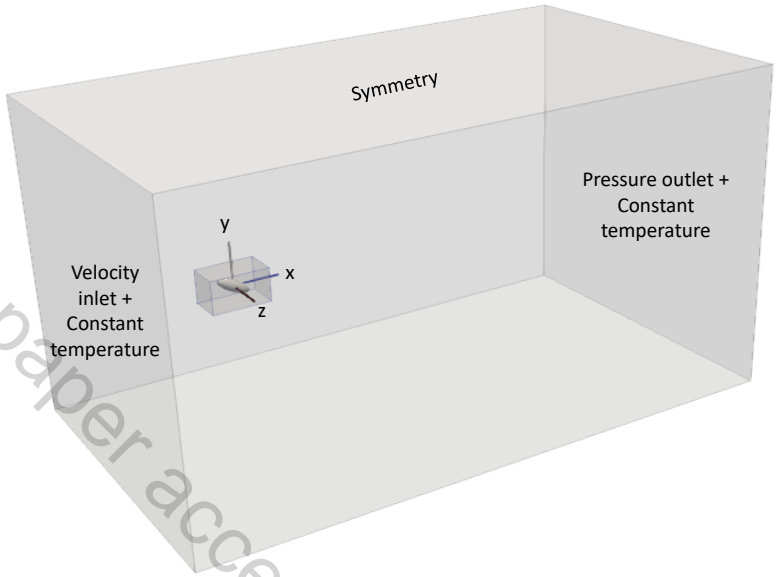

Figure 2 : Representation of the computational domain.

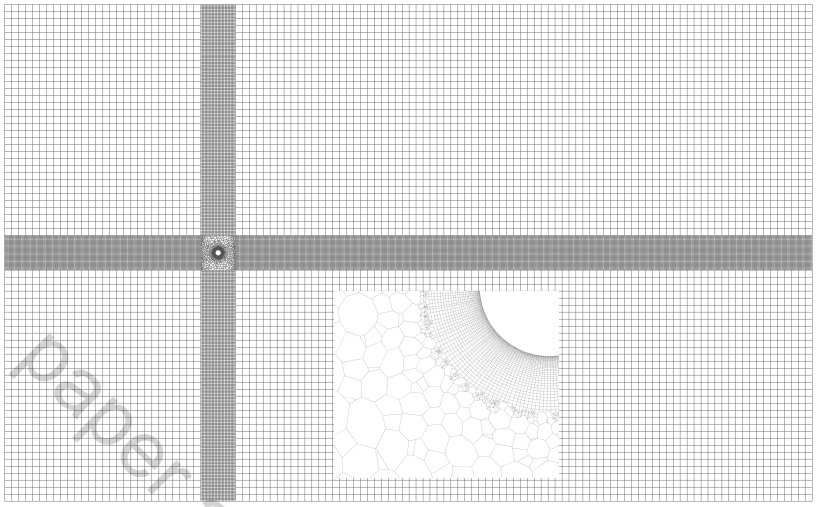

Figure 3 : Representation of the mesh on the xy-plane with a detailed view of the vicinity of the particle.

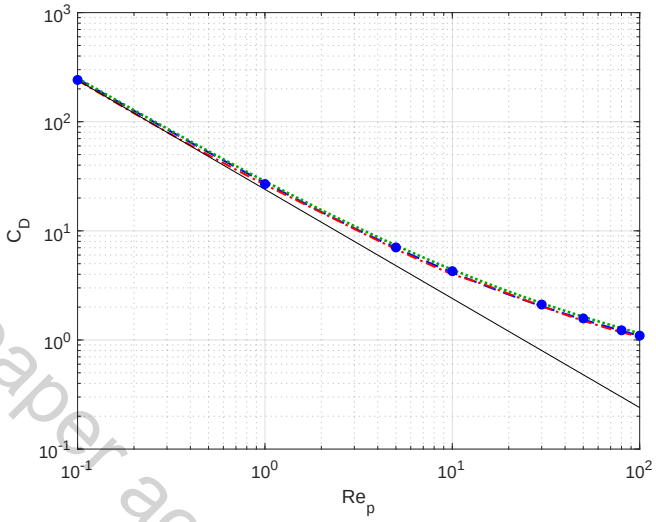

Figure 4 : Comparison between the present drag coefficients (•) and the literature correlations for a sphere : Schiller and Naumann [21] (– – –), Morsi and Alexander [22] (– · –), Haider and Levenspiel [7] (· · ·) and Stokes [23] (——).

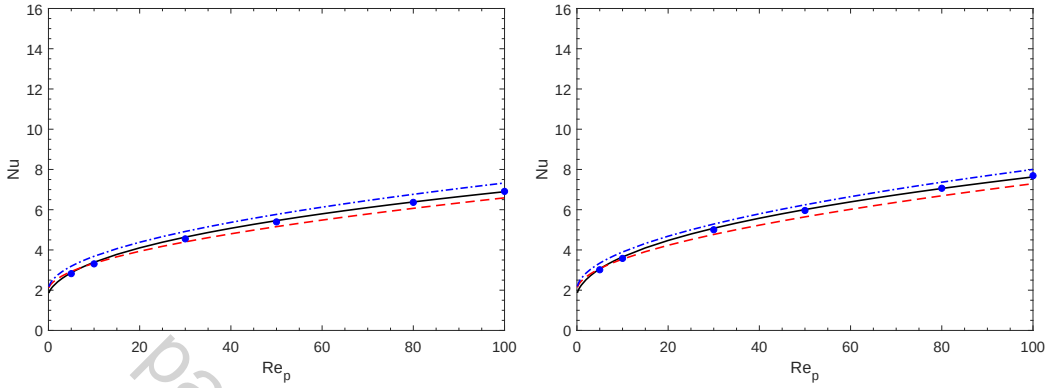

(a) $Pr = 0.7$ (b) $Pr = 1$

(c) $Pr = 4$ (d) $Pr = 7$

Figure 5 : Comparison between the present results (●) and the literature correlations for a sphere : Clift *et al.* [18] (——), Whitaker [25] (– – –) and Ranz and Marshall [24] (– · –).

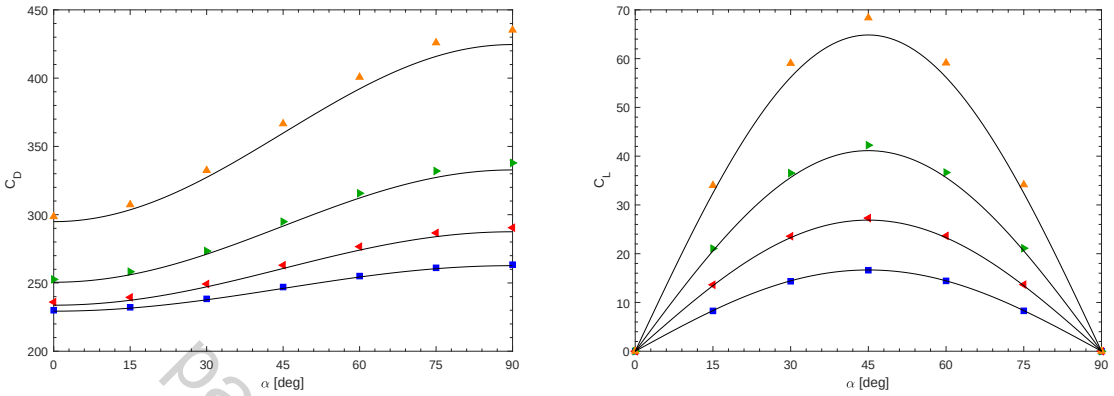

(a) C_D (b) C_L

Figure 6 : Comparison of the present force coefficients for several aspect ratios ($E = 2$ ■, $E = 3$ ◀, $E = 5$ ▶, $E = 10$ ▲) and theoretical solutions of Happel and Brenner [5] (—) at $Re_p = 0.1$.

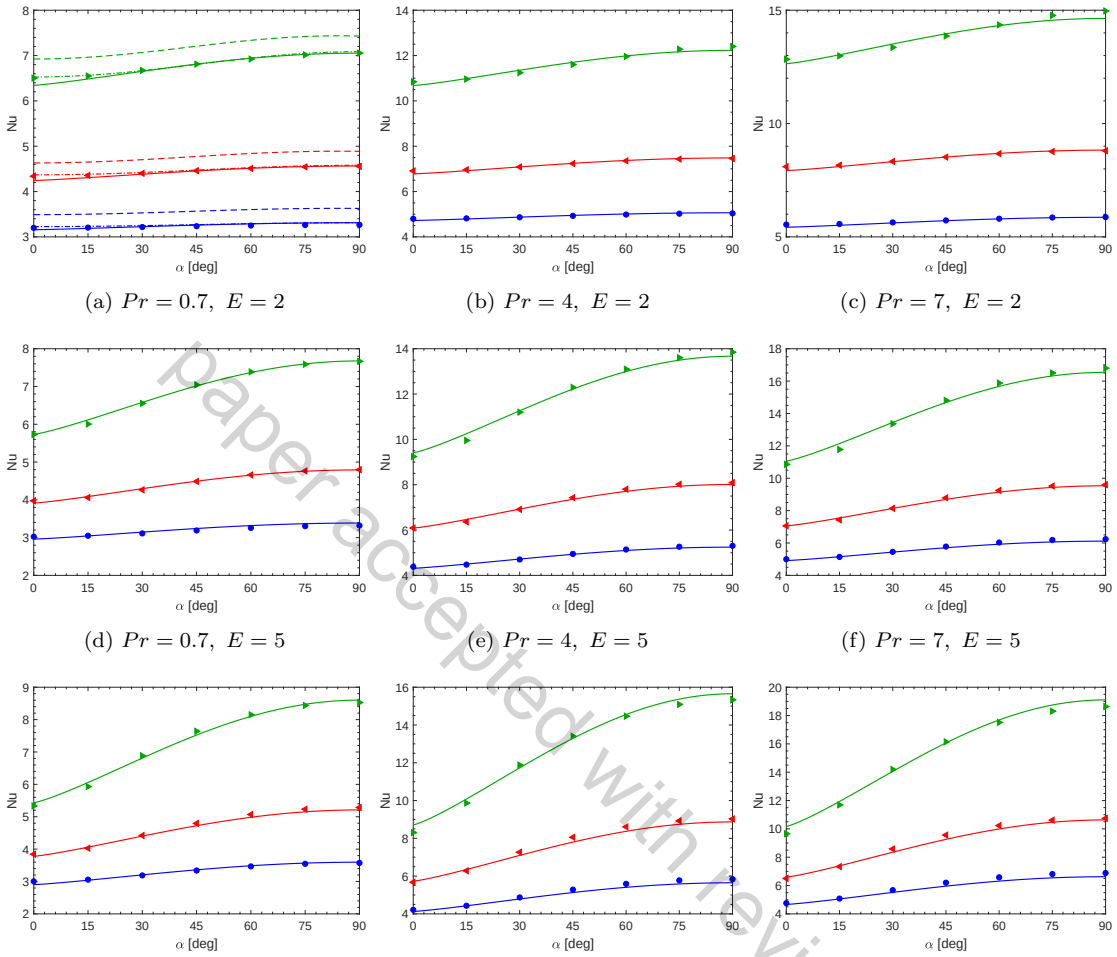

(a) $Pr = 0.7,\ E = 2$ (b) $Pr = 4,\ E = 2$ (c) $Pr = 7,\ E = 2$

(d) $Pr = 0.7,\ E = 5$ (e) $Pr = 4,\ E = 5$ (f) $Pr = 7,\ E = 5$

(g) $Pr = 0.7,\ E = 10$ (h) $Pr = 4,\ E = 10$ (i) $Pr = 7,\ E = 10$

Figure 7 : $Nu = f(\alpha)$ for different Prandtl numbers and aspect ratios at $Re_p = 10$ (●), $Re_p = 30$ (◀) and $Re_p = 100$ (▶). Solid lines correspond to the present Nu correlation, dashed lines to Ke *et al.* [16] and dash-dotted lines to Richter and Nikrityuk [13] (Fig. 7a only).

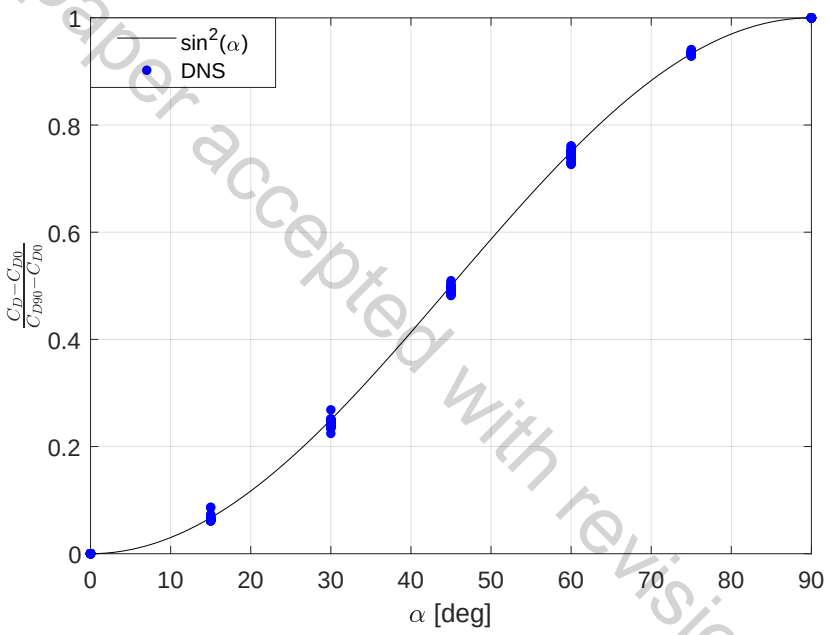

Figure 8 : Evolution of the normalised drag coefficient as a function of the angle of attack.

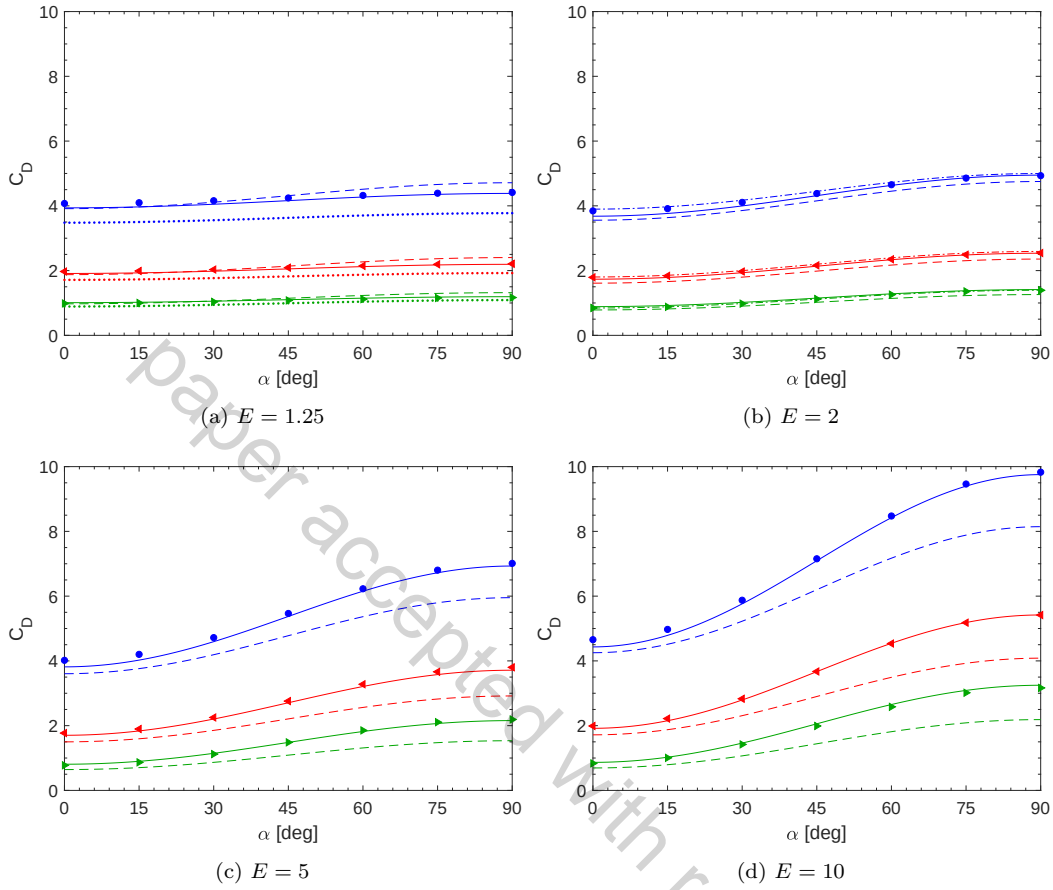

(a) $E = 1.25$ (b) $E = 2$

(c) $E = 5$ (d) $E = 10$

Figure 9 : $C_D = f(\alpha)$ for different aspect ratios at $Re_p = 10$ (●), $Re_p = 30$ (◀) and $Re_p = 100$ (▶). Solid lines correspond to the present C_D correlation, dashed lines to Ouchene *et al.* [10], dash-dotted lines to Richter and Nikrityuk [13] and dotted lines to Zastawny *et al.* [11].

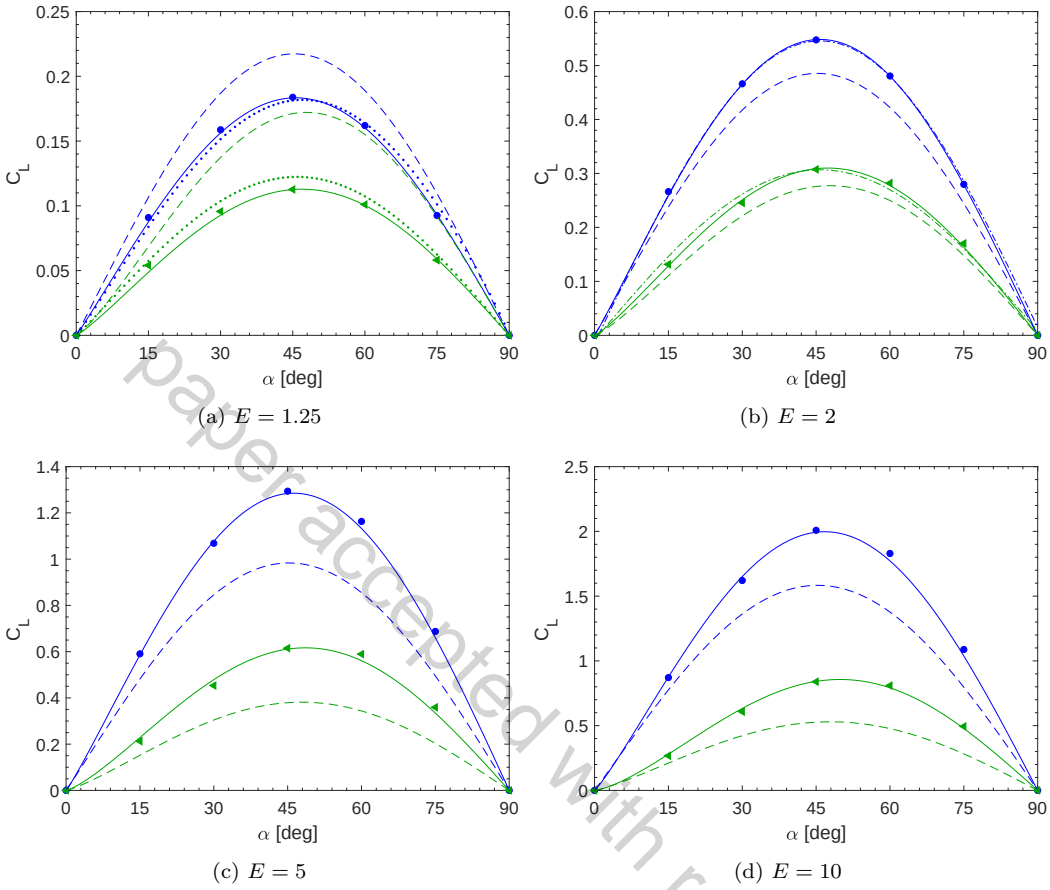

(a) $E = 1.25$ (b) $E = 2$

(c) $E = 5$ (d) $E = 10$

Figure 10 : $C_L = f(\alpha)$ for different aspect ratios at $Re_p = 10$ (●) and $Re_p = 100$ (▶). Solid lines correspond to the present C_L correlation, dashed lines to Ouchene *et al.* [10], dash-dotted lines to Richter and Nikrityuk [13] and dotted lines to Zastawny *et al.* [11].

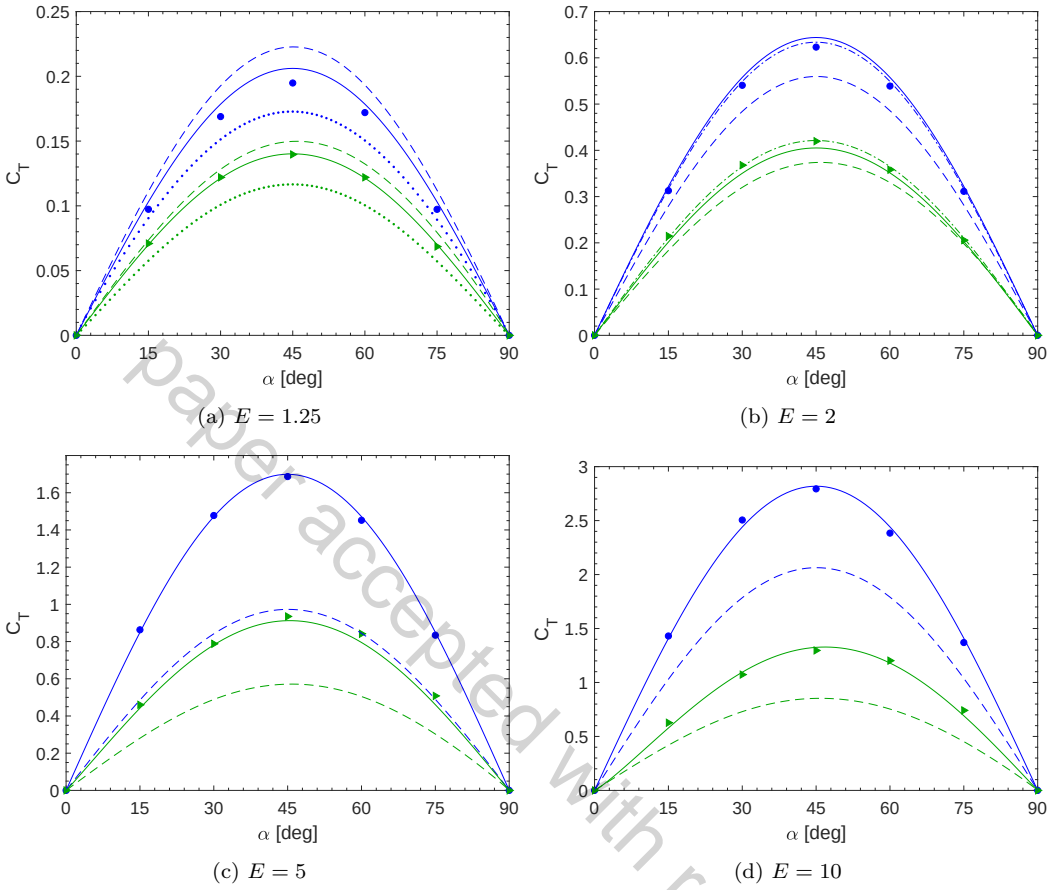

(a) $E = 1.25$ (b) $E = 2$

(c) $E = 5$ (d) $E = 10$

Figure 11 : $C_T = f(\alpha)$ for different aspect ratios at $Re_p = 10$ (●) and $Re_p = 100$ (▶). Solid lines correspond to the present C_T correlation, dashed lines to Ouchene *et al.* [10], dash-dotted lines to Richter and Nikrityuk [13] and dotted lines to Zastawny *et al.* [11].

List of Tables

Type	Grid	# cells ($\times 10^6$)	C_D	Nu	CPU time [s]	# iterations
Polyhedral	1P	2.93	1.0949	14.080	208,600	2420
	2P	1.77	1.0950	14.080	180,745	2740
	3P	1.31	1.0964	14.082	98,386	3420
Tetrahedral	1T	3.46	1.0941	14.080	331,218	3380
	2T	2.28	1.0943	14.080	269,944	3780
	3T	1.81	1.0950	14.080	185,678	4000

Table 1 : Characteristics of each tested mesh for a sphere at $Re_p = 100$ and $Pr = 7$.

	Relative deviations	
	Mean [%]	Max [%]
Schiller and Naumann [21]	2.0	3.5
Morsi and Alexander [22]	3.4	6.8
Haider and Levenspiel [7]	4.0	5.7

Table 2 : Mean and maximum deviations between the present study and the drag coefficient correlations for a sphere ($0.1 \leq Re_p \leq 100$).

	Relative deviations	
	Mean [%]	Max [%]
Clift *et al.* [18]	1.4	3.2
Ranz and Marshall [24]	5.1	9.0
Whitaker [25]	4.8	11.5

Table 3 : Mean and maximum deviations between the present study and the Nusselt number correlations for a sphere ($0.1 \leq Re_p \leq 100$ and $0.7 \leq Pr \leq 7$).

Aspect ratio E	1.25		2		3		5		10	
	C_D	C_L	C_D	C_L	C_D	C_L	C_D	C_L	C_D	C_L
Mean relative deviations [%]	0.39	1.3	0.29	0.46	0.94	1.5	1.1	2.6	1.9	5.2
Max relative deviations [%]	0.63	4.0	0.41	0.76	1.0	1.6	1.5	2.9	2.5	5.4

Table 4 : Mean and maximum deviations between the present study and the correlations of Happel and Brenner [5].

Pr	Relative deviations	
	Mean [%]	Max [%]
0.7	0.31	0.71
1	0.58	1.1
4	1.9	3.0
7	2.4	4.1

Table 5 : Mean and maximum deviations between the present study and the correlation of Clift *et al.* [18] for ellipsoids at $Re_p = 0.1$ and $1.25 \leq E \leq 10$.

E	Present simulations		Richter and Nikrityuk†[13]		Ke *et al.*† [16]	
	Mean [%]	Max [%]	Mean [%]	Max [%]	Mean [%]	Max [%]
1	1.00	5.16	-	-	3.91	5.84
1.25	0.90	4.71	-	-	4.15	6.60
2	1.02	4.10	0.70	2.94	6.83	9.55
3	1.04	3.62	-	-	-	-
5	1.19	3.79	-	-	-	-
10	1.71	5.30	-	-	-	-

Table 6 : Comparison of the present Nu correlation with the results of simulations (for $0.1 \leq Re_p \leq 100$ and $0.7 \leq Pr \leq 7$) and the existing correlations.
† The relative deviations are calculated within the range of validity of these correlations (i.e. $Re_p \geq 10$ and $Pr = 0.7$).

E	Present simulations		Ouchene *et al.* [10]		Zastawny *et al.*† [11]		Richter and Nikrityuk† [13]	
	Mean [%]	Max [%]	Mean [%]	Max [%]	Mean [%]	Max [%]	Mean [%]	Max [%]
1	2.00	3.34	0	0	-	-	-	-
1.25	1.84	3.96	3.43	9.46	13.7	19.3	-	-
2	2.00	4.85	6.02	13.0	-	-	2.31	5.60
3	1.98	5.04	12.0	27.3	-	-	-	-
5	2.13	5.03	17.1	40.5	-	-	-	-
10	1.90	4.80	19.5	48.5	-	-	-	-

Table 7 : Comparison of the present C_D correlation with the results of simulations (for $0.1 \leq Re_p \leq 100$) and the existing correlations.
† The relative deviations are calculated within the range of validity of these correlations.

E	Present simulations		Ouchene *et al.* [10]		Zastawny *et al.*† [11]		Richter and Nikrityuk† [13]	
	Mean [%]	Max [%]	Mean [%]	Max [%]	Mean [%]	Max [%]	Mean [%]	Max [%]
1.25	3.27	10.0	22.1	37.1	8.83	48.6	-	-
2	2.45	6.34	11.9	40.7	-	-	6.15	15.0
3	2.67	7.55	29.7	45.3	-	-	-	-
5	3.10	7.42	38.6	66.7	-	-	-	-
10	2.78	6.51	34.6	80.6	-	-	-	-

Table 8 : Comparison of the present C_L correlation with the results of simulations (for $0.1 \leq Re_p \leq 100$) and the existing correlations.
† The relative deviations are calculated within the range of validity of these correlations.

E	Present simulations		Ouchene *et al.* [10]		Zastawny *et al.*† [11]		Richter and Nikrityuk† [13]	
	Mean [%]	Max [%]	Mean [%]	Max [%]	Mean [%]	Max [%]	Mean [%]	Max [%]
1.25	2.66	6.63	11.3	24.6	14.0	31.2	-	-
2	2.21	6.04	12.6	22.4	-	-	0.41	1.34
3	2.06	5.51	38.9	60.9	-	-	-	-
5	1.81	9.33	69.6	94.4	-	-	-	-
10	2.34	7.82	45.3	61.3	-	-	-	-

Table 9 : Comparison of the present C_T correlations with the results of simulations (for $1 \leq Re_p \leq 100$) and the existing correlations.
† The relative deviations are calculated within the range of validity of these correlations.

Highlights:

- Drag, lift, torque and Nusselt number are studied numerically for prolate spheroids
- New correlations are derived from the numerical simulations
- The correlations take into account the orientation of the spheroidal particles
- The correlations are valid from the Stokes regime up to Reynolds numbers of 100
- The local use of a polyhedral mesh allowed a faster convergence

The authors declare no conflict of interest.